We are IntechOpen, the world's leading publisher of Open Access books Built by scientists, for scientists

6,900
Open access books available

185,000
International authors and editors

200M
Downloads

154
Countries delivered to

Our authors are among the

TOP 1%
most cited scientists

12.2%
Contributors from top 500 universities

CLARIVATE ANALYTICS

BOOK CITATION INDEX

INDEXED

WEB OF SCIENCE™

Selection of our books indexed in the Book Citation Index
in Web of Science™ Core Collection (BKCI)

Interested in publishing with us?
Contact book.department@intechopen.com

Numbers displayed above are based on latest data collected.
For more information visit www.intechopen.com

Techniques for Calculating Two Interesting Types of Dielectric Materials in Straight Rectangular Waveguides and Their Applications

Zion Menachem

Abstract

This chapter presents two interesting types of dielectric materials in the straight rectangular waveguides. Five examples of the different discontinuous cross sections and complementary shapes will demonstrate. We will introduce in all case the effective technique to calculate the dielectric profile in the cross section. The first type will demonstrate where the dielectric material is located in the center of the cross section. The second type will demonstrate where the hollow core is located in the center of the cross section in the case of the hollow waveguide. The two different types are complementary shapes for two different applications. The proposed techniques relate to the method based on Laplace and Fourier transforms and the inverse Laplace and Fourier transforms. The method is based also on Fourier transform, thus we need use with the image method to calculate the dielectric profile in the cross section. The image method and periodic replication are needed for fulfilling the boundary condition of the metallic waveguide. The applications are useful for straight waveguides in millimeter regimes, in the cases where the dielectric profile is located in the center of the cross section, for cases where the hollow rectangle is located in the center of the cross section, and also for complicated and discontinuous profiles in the cross section.

Keywords: wave propagation, dielectric profiles, rectangular waveguides, dielectric materials

1. Introduction

Review of numerical and approximate methods for the modal analysis of general optical dielectric waveguides with emphasis on recent developments has been published [1]. In this review, interesting methods are given such as, the finite-difference and the finite-element methods. Review of numerical methods for the analysis of the homogeneous and inhomogeneous, isotropic and anisotropic, microwave and optical dielectric waveguides with arbitrarily-shaped cross sections has been published [2]. The main approaches as the integral equations, finite difference, and finite element have been discussed.

A fundamental and accurate approach to compute the attenuation of electromagnetic waves propagating has been proposed [3]. The propagation constant was found by substituting the values of transverse wave numbers into the dispersion relation. A Green's dyadic for describing the propagating electromagnetic waves in a rectangular dielectric waveguide has been developed [4]. The use of Green's dyadic developed in order to calculate the effect of small perturbations upon the system.

An analytical method for solution of one-dimensional optical systems, based on the differential transfer matrices has been presented [5]. An approach to solve the problem of the propagation of electromagnetic waves in unidimensional media with an arbitrary variation of their dielectric permittivity has been proposed [6]. This method was deduced from the Maxwell equations with a minimum of approximations and allows a full vectorial description of both the electric and magnetic fields through the direct calculation of their cartesian coordinates. The equations permit the simulation of materials with a continuous variation of their dielectric permittivity without approximating them by discontinuous layered media, reducing so the computational effort of the models.

An analytical method for solution of non-homogeneous anisotropic optical systems, based on the extension of transfer matrices into differential form has been presented [7]. This approach can be used for exact calculation of various functions including reflection and transmission coefficients, band structures and bound states. A full-wave analysis of lossy dielectric waveguides using a hybrid vector finite element method has been presented [8]. The direct matrix solution technique with minimum degree of reordering has been combined with the modified Lanczos algorithm to solve for the resultant sparse generalized eigenmatrix equation efficiently.

Three-dimensional finite-element method with edge elements for electromagnetic waveguide discontinuities has been proposed [9]. This paper shows that the finite-element method using edge elements succeeds in suppressing spurious solutions and moreover that this method succeeds in the analysis of three-dimensional electromagnetic waveguide problems with metal wedges. An analytical approach based on scalar wave approximation to estimate the modal dispersion characteristics and cutoff condition of an optical waveguide has been presented [10]. This approach has an arbitrary and uniform core cross-section. The structure represents the core of a circular waveguide which is compressed at both the ends of a diameter.

Propagation characteristics of modes in some rectangular waveguides using the finite-difference time-domain method have been studied [11]. The method in this paper was used to determine the modal characterization of rectangular waveguide structures by means of a least-square non-linear fitting to a theoretical modal expansion. Wave propagation along a rectangular waveguide with slowly varying width has been investigated [12] with the help of field theory and approximate circuit theory. Many properties of the modulated periodic structure, e.g., the frequency dependence of the propagation constant, group and phase velocities, and the electric field axial variation for the fundamental space harmonic and its filter-like property have been investigated.

A method for measuring samples using a partially-filled waveguide has been presented [13]. A mode-matching technique was used to determine the fields in the three regions. An advantageous finite element method for the rectangular waveguide problem has been developed [14] by which complex propagation characteristics may be obtained for arbitrarily shaped waveguide.

A method has been introduced for the frequency domain analysis of arbitrary longitudinally inhomogeneous waveguides [15]. The integral equations of the longitudinally inhomogeneous waveguides, converted from their differential equations, were solved using the method of moments. A method has been introduced for the frequency domain analysis of arbitrarily loaded lossy and dispersive

nonuniform transmission lines [16]. In this method, all distributed primary parameters of the line and also the voltage and current distribution along the line were considered as a Taylor's series.

A technique based on the two-dimensional Fourier transform has been presented [17] and applied to the study of nonlinear wave propagation phenomena in one-dimensional, finite, nonlinear transmission lines.

A method for calculating the modes of arbitrarily shaped dielectric waveguides has been presented [18]. It consists of expanding the field in a two-dimensional Fourier series. The expansion has been used to convert the scalar wave equation into a matrix eigenvalue equation. A transfer matrix function for the analysis of electromagnetic wave propagation along the straight dielectric waveguide with arbitrary profiles has been proposed [19]. This method is based on the Laplace and Fourier transforms and the inverse Laplace and Fourier transforms.

2. Complicated and discontinuous profiles in the cross section

In this chapter, we present some examples of dielectric structures as shown in **Figure 1a–e**. The method is based on Fourier transform, thus we need use with the image method and periodic replication for fulfilling the boundary conditions of the metallic waveguide. We relate also to the complementary shapes for different applications. The periodicity and the symmetry properties are chosen to force the boundary conditions at the location of the walls in real problem, by extending the
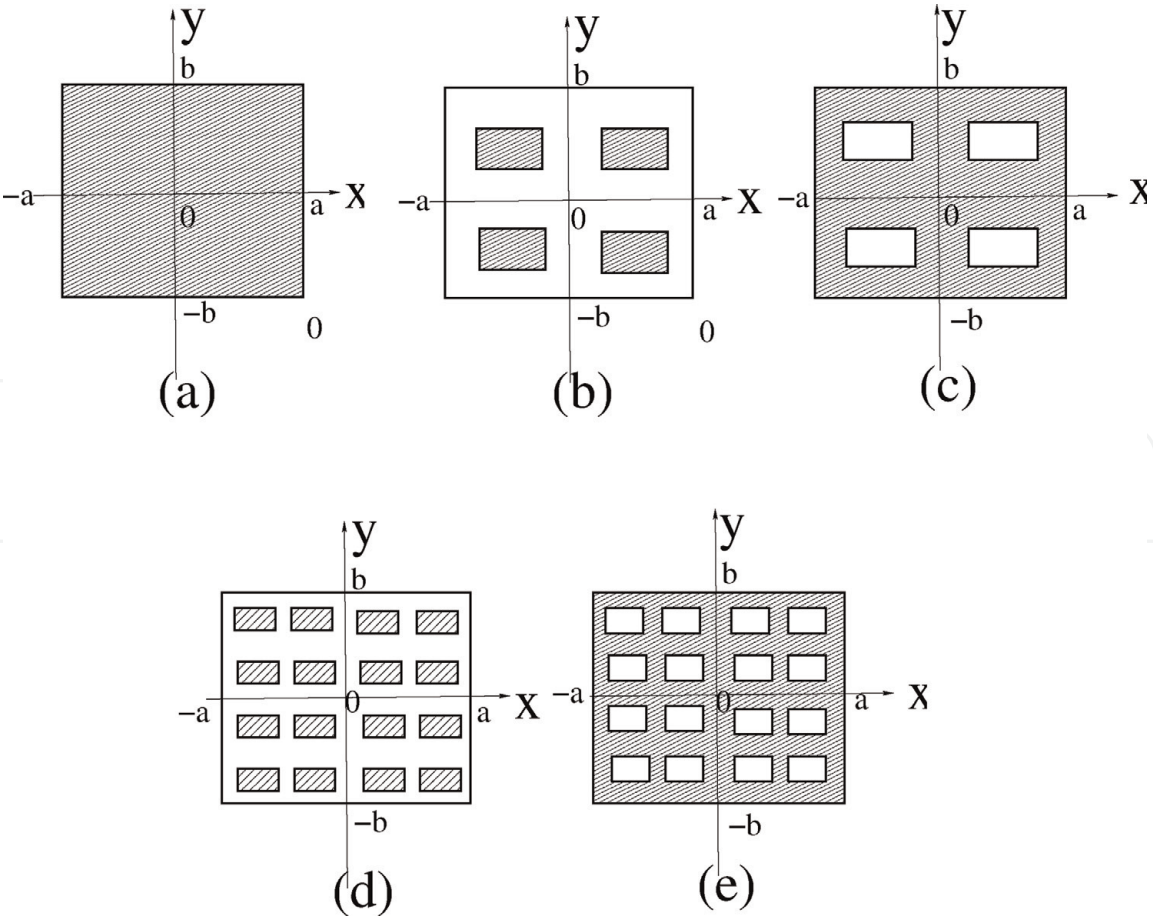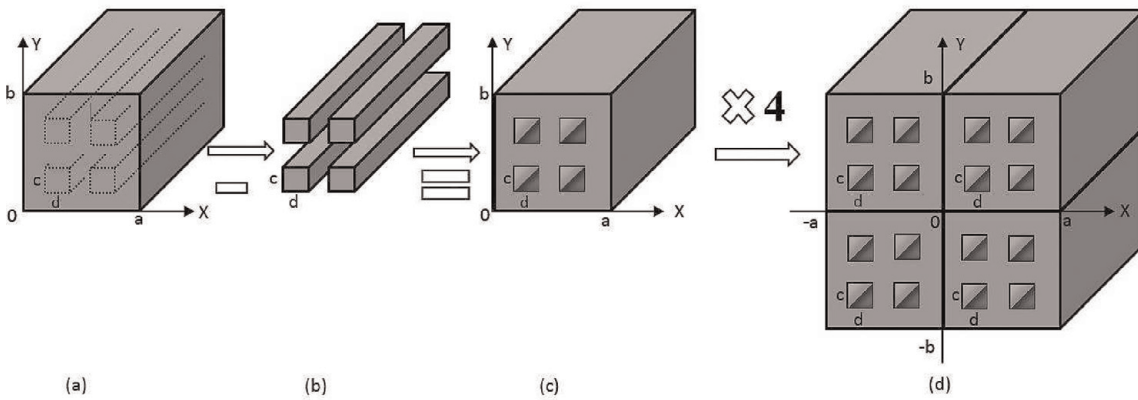

Figure 1.
The image method and periodic replication for five examples. (a). The cross section entirely filled with the dielectric material, (b). The dielectric material is located in the center of the cross section, (c). The hollow waveguide where the hollow rectangle is located in the center of the cross section, (d). The cross section consists with four dielectric profiles, and (e). The hollow waveguide with four hollow rectangles.
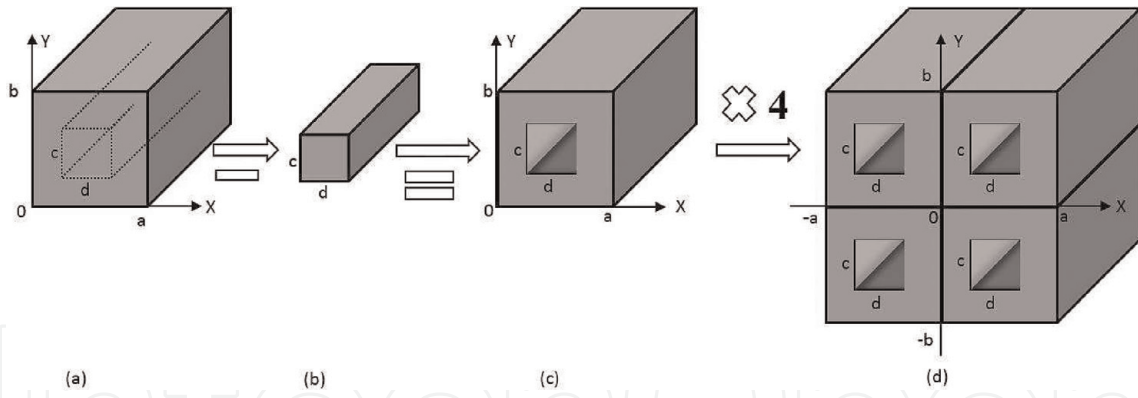
Figure 2.
Example of receiving a hollow waveguide where the hallow rectangle is located in the center (c) by substracting the waveguide with dielectric material located at the center of the cross section (b) from the waveguide entirely filled with the dielectric material (a), and by using the image method (d).

Figure 3.
Example of receiving a hollow waveguide with four hollow rectangles (c) by substracting the four dielectric rectangles (b) from the waveguide entirely filled with the dielectric material (a), and by using the image method (d).

waveguide region ($0 \leq x \leq a$, and $0 \leq y \leq b$) to a fourfold larger regions ($-a \leq x \leq a$, and $-b \leq y \leq b$), as larger regions, as described in [19]. **Figure 1a** shows the case where the cross section entirely filled with the dielectric material. The dielectric material in **Figure 1b** is located in the center of the cross section. **Figure 1c** represents the hollow waveguide where the hollow rectangle is located in the center of the cross section. The cross section of **Figure 1d** consists with four dielectric profiles in the cross section. **Figure 1e** represents the hollow waveguide with four hollow rectangles.

Note that the geometries from **Figure 1a–e** become more complex. Calculating of the dielectric profile for **Figure 1a** is the simplest and for **Figure 1e** is the most complicated in relation to the examples described in these examples. The integrals of the dielectric profiles of the geometries described in **Figure 1a** and **b** can be calculated by analytical form and without solving numerical form. The calculation of the dielectric profile for the geometry of **Figure 1c** for a hollow rectangle in the center is interesting in the case of hollow waveguide, but it is more complicated than the case of **Figure 1b**. Therefore, in this case we should calculate the dielectric profile by substracting the dielectric profile of **Figure 1b** from the dielectric profile of **Figure 1a**. The calculation of the integrals of the dielectric profiles for the geometries depicted in **Figure 1d** and **e** are already more complicated, and in such cases the proposed techniques require that the integrals be solved numerically. We will explain the proposed technique for calculating the dielectric profile for each case.

Figure 2c represents an example of receiving a hollow waveguide where the hollow rectangle is located in the center by substracting the waveguide with dielectric material

located at the center of the cross section (**Figure 2b**) from the waveguide entirely filled with the dielectric material (**Figure 2a**), and by using the image method (**Figure 2d**). **Figure 3c** represents an example of receiving a hollow waveguide with four hollow rectangles by substracting the four dielectric rectangles (**Figure 3b**) from the waveguide entirely filled with the dielectric material (**Figure 3a**), and by using with the image method (**Figure 3d**).

3. The analytical technique to calculate the dielectric profiles

This section presents a technique to calculate the dielectric profile for the two inhomogeneous geometries of the cross section, as shown in **Figure 4a** and **b**.

Figure 4a and **b** show the cross section of **Figure 1b** and **c**, respectively, with the relevant parameters. These figures represent two examples of the complementary shapes in the cross section. The periodic replication is shown in **Figure 4c** by using with the image method. The dielectric material in **Figure 4a** is located in the center of the cross section. The hollow rectangle in **Figure 4b** is located in the center of the cross section in the case of the hollow waveguide.

The dielectric profile $g(x, y)$ is given according to $\epsilon(x, y) = \epsilon_0(1 + g(x, y))$. If $g(x, y) = g_0$ and $\epsilon_r(x, y) = \epsilon_r$, then we obtain that g0 = $\epsilon_r - 1$. According to **Figure 4a** and **c** for $g(x, y) = g_0$, we obtain

$$
\begin{aligned}
g(n, m) =& \frac{g_0}{4ab} \int_{-a}^{a} dx \int_{-b}^{b} \exp\left[-j(k_x x + k_y y)\right] dy \\
=& \frac{g_0}{4ab} \left\{ \int_{x_{11}}^{x_{12}} dx \int_{y_{11}}^{y_{12}} \exp\left[-j(k_x x + k_y y)\right] dy + \int_{-x_{12}}^{-x_{11}} dx \int_{y_{11}}^{y_{12}} \exp\left[-j(k_x x + k_y y)\right] dy \right. \\
&\left. + \int_{-x_{12}}^{-x_{11}} dx \int_{-y_{12}}^{-y_{11}} \exp\left[-j(k_x x + k_y y)\right] dy + \int_{x_{11}}^{x_{12}} dx \int_{-y_{12}}^{-y_{11}} \exp\left[-j(k_x x + k_y y)\right] dy \right\} \\
=& \frac{g_0}{4ab} \left\{ \int_{x_{11}}^{x_{12}} dx \int_{y_{11}}^{y_{12}} \exp\left[-j(k_x x + k_y y)\right] dy + \int_{x_{12}}^{x_{11}} - dx \int_{y_{11}}^{y_{12}} \exp\left[-j(-k_x x + k_y y)\right] dy \right. \\
&\left. + \int_{x_{12}}^{x_{11}} - dx \int_{y_{12}}^{y_{11}} - \exp\left[-j(-k_x x - k_y y)\right] dy + \int_{x_{11}}^{x_{12}} dx \int_{y_{12}}^{y_{11}} - \exp\left[-j(k_x x - k_y y)\right] dy \right\} \\
=& \frac{g_0}{4ab} \left\{ \int_{x_{11}}^{x_{12}} \exp\left[j(k_x x)\right] dx \int_{y_{11}}^{y_{12}} \exp\left[j(k_y y)\right] dy + \int_{x_{11}}^{x_{12}} \exp\left[j(k_x x)\right] dx \int_{y_{11}}^{y_{12}} \exp\left[-j(k_y y)\right] dy \right. \\
&\left. + \int_{x_{11}}^{x_{12}} \exp\left[-j(k_x x)\right] dx \int_{y_{11}}^{y_{12}} \exp\left[j(k_y y)\right] dy + \int_{x_{11}}^{x_{12}} \exp\left[-j(k_x x)\right] dx \int_{y_{11}}^{y_{12}} \exp\left[-j(k_y y)\right] dy \right\} \\
=& \frac{g_0}{4ab} \left\{ \int_{x_{11}}^{x_{12}} dx \int_{y_{11}}^{y_{12}} \exp\left[-j(k_x x + k_y y)\right] dy + \int_{x_{11}}^{x_{12}} dx \int_{y_{11}}^{y_{12}} \exp\left[j(k_x x - k_y y)\right] dy \right. \\
&\left. + \int_{x_{11}}^{x_{12}} dx \int_{y_{11}}^{y_{12}} \exp\left[j(k_x x + k_y y)\right] dy + \int_{x_{11}}^{x_{12}} dx \int_{y_{11}}^{y_{12}} \exp\left[-j(k_x x - k_y y)\right] dy \right\} \\
=& \frac{g_0}{2ab} \left\{ \int_{x_{11}}^{x_{12}} \left(\exp\left(jk_x x\right) + \exp\left(-jk_x x\right) \right) dx \int_{y_{11}}^{y_{12}} \cos\left(k_y y\right) dy \right\},
\end{aligned}
$$

(1)

5
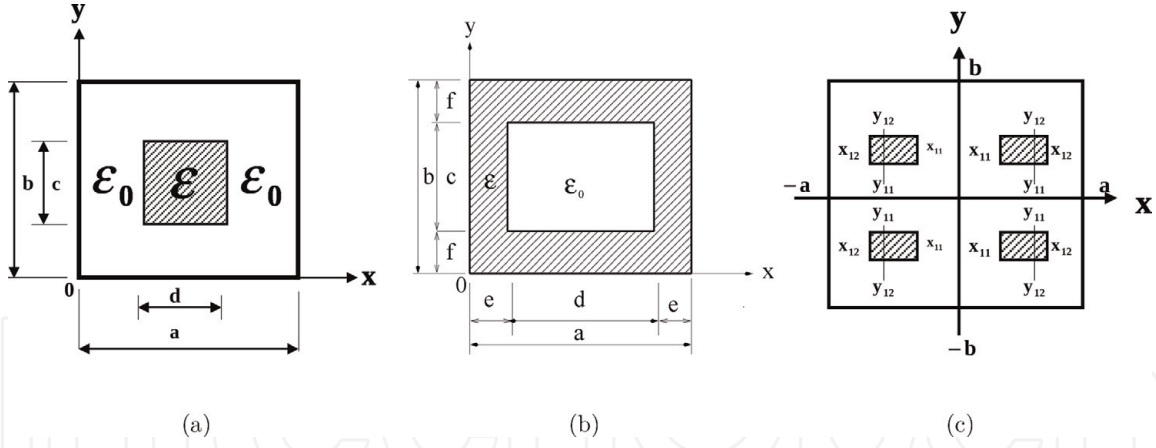
Figure 4.
Two examples of the complementary shapes of profiles in the cross section and the periodic replication, (a). The dielectric material is located in the center of the cross section with the relevant parameters of Figure 1b, (b). The hollow rectangle is located in the center of the cross section in the case of the hollow waveguide with the relevant parameters of Figure 1c, (c). The periodic replication according to the image method.

where $k_x = (n\pi x)/a$, and $k_y = (m\pi y)/b$. The derivatives of the dielectric profile are calculated according to $g_x(x, y) = (1/\epsilon(x, y))(d\epsilon(x, y)/dx)$, and $g_y(x, y) = (1/\epsilon(x, y))(d\epsilon(x, y)/dy)$, where $\epsilon(x, y) = \epsilon_0(1 + g(x, y))$.

For the cross section as shown in **Figure 4a** and according to **Figure 4c**, the center of the dielectric rectangle is located at (a/2, b/2). According to **Figure 4a** and **c**, the Fourier components of the dielectric profile are given by

$$
g_1(n, m) = \begin{cases}
\dfrac{g_0}{4ab}(4cd) & n = 0, m = 0 \\[3mm]
\dfrac{g_0}{4ab}\left(\dfrac{8d}{k_{0y}m}\sin\left(\dfrac{k_{0y}mc}{2}\right)\cos\left(\dfrac{k_{0y}mb}{2}\right)\right) & n = 0, m \neq 0 \\[3mm]
\dfrac{g_0}{4ab}\left(\dfrac{8c}{k_{0x}n}\sin\left(\dfrac{k_{0x}nd}{2}\right)\cos\left(\dfrac{k_{0x}na}{2}\right)\right) & n \neq 0, m = 0 \\[3mm]
\dfrac{g_0}{4ab}\left(\dfrac{16}{k_{0x}k_{0y}nm}\sin\left(\dfrac{k_{0x}nd}{2}\right)\cos\left(\dfrac{k_{0x}na}{2}\right)\sin\left(\dfrac{k_{0y}mc}{2}\right)\cos\left(\dfrac{k_{0y}mb}{2}\right)\right) & n \neq 0, m \neq 0
\end{cases}
$$

$$(2)$$

Similarly, for the cross section entirely filled with the dielectric material as shown in **Figure 1a**, the Fourier components of the dielectric profile are given by

$$
g_2(n, m) = \begin{cases}
g_0 & n = 0, m = 0 \\[3mm]
\dfrac{g_0}{4ab}\left(\dfrac{8a}{k_{0y}m}\sin\left(\dfrac{k_{0y}mb}{2}\right)\cos\left(\dfrac{k_{0y}mb}{2}\right)\right) & n = 0, m \neq 0 \\[3mm]
\dfrac{g_0}{4ab}\left(\dfrac{8b}{k_{0x}n}\sin\left(\dfrac{k_{0x}na}{2}\right)\cos\left(\dfrac{k_{0x}na}{2}\right)\right) & n \neq 0, m = 0 \\[3mm]
\dfrac{g_0}{4ab}\left(\dfrac{16}{k_{0x}k_{0y}nm}\sin\left(\dfrac{k_{0x}na}{2}\right)\cos\left(\dfrac{k_{0x}na}{2}\right)\sin\left(\dfrac{k_{0y}mb}{2}\right)\cos\left(\dfrac{k_{0y}mb}{2}\right)\right) & n \neq 0, m \neq 0
\end{cases}
$$

$$(3)$$

The Fourier components of the dielectric profile ($g(n, m)$) of the hollow rectangular waveguide with the hollow rectangle in the center of the cross section

(**Figure 4b**) are calculated by subtracting the dielectric profile of the waveguide with the dielectric material in the core ($g_1(n, m)$) as shown in **Figure 4a** from the dielectric profile of the waveguide entirely with the dielectric material ($g_2(n, m)$) as shown in **Figure 1a**. Namely, the Fourier components of the dielectric profile ($g(n, m)$) are given by $g_2(n, m) - g_1(n, m)$. The two different types of the cross sections are complementary shapes for two different applications.

4. The numerical technique to calculate the dielectric profiles

4.1 Calculation of the dielectric profile according to the ω_ε function

Figure 5a and **b** show the cross section of **Figure 1d** and **e**, respectively, with the relevant parameters. These figures represent two examples of the complementary shapes in the cross section. The cross section consists with four dielectric profiles as shown in **Figure 5a**. The hollow waveguide with four hollow rectangles is shown in **Figure 5b**. The centers of the first, the second, the third and the firth dielectric rectangles in **Figure 5a** and hollow rectangles in **Figure 5b** are located at the points (a/4, b/4), (3a/4, b/4), (a/4, 3b/4), and (3a/4, 3b/4), respectively. The calculation of the elements of the matrix in **Figure 5b** is already more complicated. Thus, the Fourier components of the dielectric profile ($g(n, m)$) of the hollow waveguide with four hollow rectangles in **Figure 5b** are calculated by subtracting the dielectric profile of the cross section with four dielectric profiles in **Figure 5a** from the dielectric profile of the waveguide entirely with the dielectric material ($g_2(n, m)$) as shown in **Figure 1a**, and according to Eq. (3).

In order to calculate the elements of the dielectric profiles of the inhomogeneous geometry of the cross section in **Figure 5a**, we can use with the ω_ε function [20], as shown in **Figure 6**. The ω_ε function is defined as $\omega_\varepsilon(r) = C_\varepsilon \exp\left[-\varepsilon^2/(\varepsilon^2 - |r|^2)\right]$ for $|r| > \varepsilon$, where C_ε is a constant, and $\int \omega_\varepsilon(r)dr = 1$. In the limit $\varepsilon \to 0$, the ω_ε function is shown in **Figure 6**.

(a)   (b)
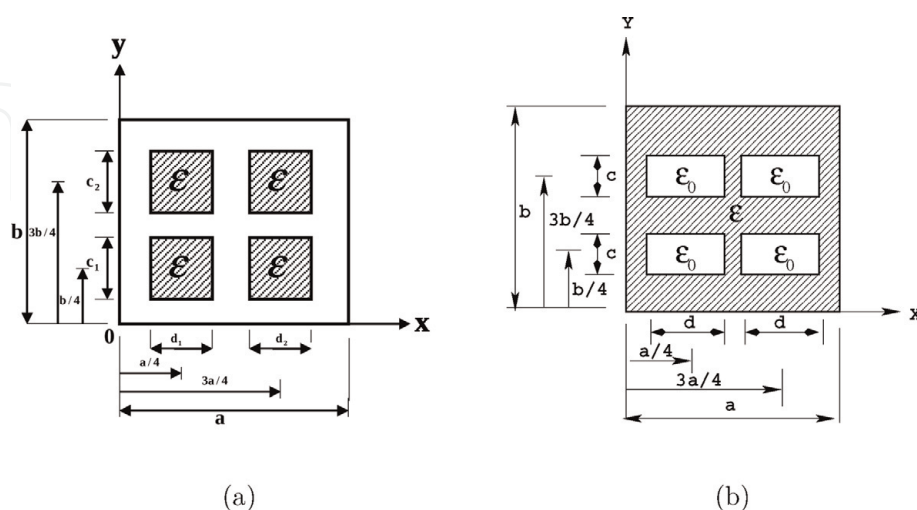
Figure 5.
*Two examples of the complementary shapes of profiles in the cross section and their relevant parameters. The centers of the first, the second, the third and the firth rectangles are located at the points (a/4, b/4), (3a/4, b/4), (a/4, 3b/4), and (3a/4, 3b/4), respectively: (a) the cross section consists with four dielectric profiles with the relevant parameters of **Figure 1d**; (b) the hollow waveguide with four hollow rectangles with the relevant parameters of **Figure 1e**.*
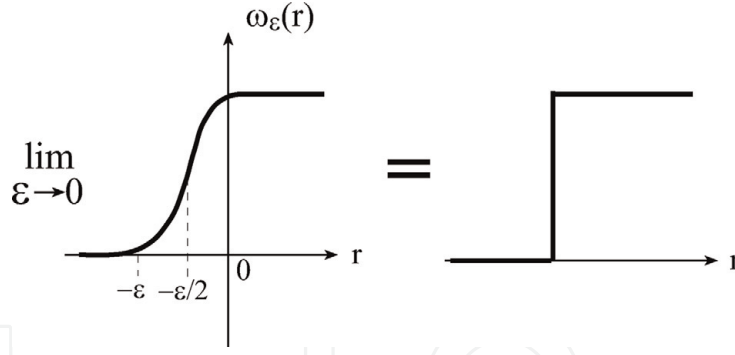
Figure 6.
The ω_ε function to calculate the elements of the dielectric profiles of the inhomogeneous geometry.

4.2 The technique based on ω_ε function for the inhomogeneous cross section

It is good idea to calculate the dielectric profile of **Figure 4a** again, by using the ω_ε function, and before considering to the more complicated geometry as shown in **Figure 5a**. The second way to calculate the dielectric profile of **Figure 4a** is given according to the ω_ε function, where the dielectric profile is located at (a/2, b/2) and is given by

$$g(x) = \begin{cases} g_0 \exp\left(1 - g_1(x)\right) & (a - d - \varepsilon)/2 \leq x < (a - d + \varepsilon)/2 \\ \\ g_0 & (a - d + \varepsilon)/2 < x < (a + d - \varepsilon)/2 \\ \\ g_0 \exp\left(1 - g_2(x)\right) & (a + d - \varepsilon)/2 \leq x < (a + d + \varepsilon)/2 \\ \\ 0 & else \end{cases}, \qquad (4)$$

and

$$g(y) = \begin{cases} g_0 \exp\left(1 - g_3(y)\right) & (b - c - \varepsilon)/2 \leq y < (b - c + \varepsilon)/2 \\ \\ g_0 & (b - c + \varepsilon)/2 < y < (b + c - \varepsilon)/2 \\ \\ g_0 \exp\left(1 - g_4(y)\right) & (b + c - \varepsilon)/2 \leq y < (b + c + \varepsilon)/2 \\ \\ 0 & else \end{cases}, \qquad (5)$$

where

$$g_1(x) = \frac{\varepsilon^2}{\varepsilon^2 - [x - (a - d + \varepsilon)/2]^2}, \quad g_2(x) = \frac{\varepsilon^2}{\varepsilon^2 - [x - (a + d - \varepsilon)/2]^2},$$

$$g_3(y) = \frac{\varepsilon^2}{\varepsilon^2 - [y - (b - c + \varepsilon)/2]^2}, \quad g_4(y) = \frac{\varepsilon^2}{\varepsilon^2 - [y - (b + c - \varepsilon)/2]^2}.$$

Similarly, we can calculate the rectangular dielectric profile according to the location of the profile in the cross section of the waveguide.

The elements of the matrix in Fourier space of the inhomogeneous geometry described in **Figure 4a** are given in the case of b ≠ c by

$$g(n,m) = \frac{g_0}{ab} \left\{ \int_{(a-d-\varepsilon)/2}^{(a-d+\varepsilon)/2} \exp\left(1 - g_1(x)\right) \cos\left(\frac{n\pi x}{a}\right) dx \right.$$

$$+ \int_{(a-d+\varepsilon)/2}^{(a+d-\varepsilon)/2} \cos\left(\frac{n\pi x}{a}\right) dx + \left. \int_{(a+d-\varepsilon)/2}^{(a+d+\varepsilon)/2} \exp\left(1 - g_2(x)\right) \cos\left(\frac{n\pi x}{a}\right) dx \right\}$$

(6)

$$\left\{ \int_{(b-c-\varepsilon)/2}^{(b-c+\varepsilon)/2} \exp\left(1 - g_3(y)\right) \cos\left(\frac{m\pi y}{b}\right) dy \right.$$

$$+ \int_{(b-c+\varepsilon)/2}^{(b+c-\varepsilon)/2} \cos\left(\frac{m\pi y}{b}\right) dy + \left. \int_{(b+c-\varepsilon)/2}^{(b+c+\varepsilon)/2} \exp\left(1 - g_4(y)\right) \cos\left(\frac{m\pi y}{b}\right) dy \right\}.$$

4.3 The technique based on ω_ε function for the inhomogeneous cross section

Figure 5a shows the cross section where the centers of the first, the second, the third and the firth rectangles are located at the points (a/4, b/4), (3a/4, b/4), (a/4, 3b/4), and (3a/4, 3b/4), respectively, and for ϵ_r = 1.1, 1.2, 1.3 and 1.4, respectively. We assume for simplicity that $d_1 = d_2 = d$ and $c_1 = c_2 = c$, according to **Figure 5a**. The dielectric profile of **Figure 5a** is given according to the ω_ε function by

$$g(x) = \begin{cases} g_0 \exp\left(1 - q_1(x)\right) & ((a/2) - d_1 - \varepsilon)/2 \leq x < ((a/2) - d_1 + \varepsilon)/2 \\ g_0 & ((a/2) - d_1 + \varepsilon)/2 < x < ((a/2) + d_1 - \varepsilon)/2 \\ g_0 \exp\left(1 - q_2(x)\right) & ((a/2) + d_1 - \varepsilon)/2 \leq x < ((a/2) + d_1 + \varepsilon)/2 \\ g_0 \exp\left(1 - q_3(x)\right) & ((3a/2) - d_2 - \varepsilon)/2 \leq x < ((3a/2) - d_2 + \varepsilon)/2, \\ g_0 & ((3a/2) - d_2 + \varepsilon)/2 < x < ((3a/2) + d_2 - \varepsilon)/2 \\ g_0 \exp\left(1 - q_4(x)\right) & ((3a/2) + d_2 - \varepsilon)/2 \leq x < ((3a/2) + d_2 + \varepsilon)/2 \\ 0 & else \end{cases}$$ (7)

and

$$g(y) = \begin{cases} g_0 \exp\left(1 - q_5(y)\right) & ((b/2) - c_1 - \varepsilon)/2 \leq y < ((b/2) - c_1 + \varepsilon)/2 \\ g_0 & ((b/2) - c_1 + \varepsilon)/2 < y < ((b/2) + c_1 - \varepsilon)/2 \\ g_0 \exp\left(1 - q_6(y)\right) & ((b/2) + c_1 - \varepsilon)/2 \leq y < ((b/2) + c_1 + \varepsilon)/2 \\ g_0 \exp\left(1 - q_7(y)\right) & ((3b/2) - c_2 - \varepsilon)/2 \leq y < ((3b/2) - c_2 + \varepsilon)/2, \\ g_0 & ((3b/2) - c_2 + \varepsilon)/2 < y < ((3b/2) + c_2 - \varepsilon)/2 \\ g_0 \exp\left(1 - q_8(y)\right) & ((3b/2) + c_2 - \varepsilon)/2 \leq y < ((3b/2) + c_2 + \varepsilon)/2 \\ 0 & else \end{cases}$$ (8)

where

$$q_1(x) = \frac{\varepsilon^2}{\varepsilon^2 - [x - ((a/2) - d_1 + \varepsilon)/2]^2}, \quad q_2(x) = \frac{\varepsilon^2}{\varepsilon^2 - [x - ((a/2) + d_1 - \varepsilon)/2]^2},$$

$$q_3(x) = \frac{\varepsilon^2}{\varepsilon^2 - [x - ((3a/2) - d_2 + \varepsilon)/2]^2}, \quad q_4(x) = \frac{\varepsilon^2}{\varepsilon^2 - [x - ((3a/2) + d_2 - \varepsilon)/2]^2}$$

$$q_5(y) = \frac{\varepsilon^2}{\varepsilon^2 - [y - ((b/2) - c_1 + \varepsilon)/2]^2}, \quad q_6(y) = \frac{\varepsilon^2}{\varepsilon^2 - [y - ((b/2) + c_1 - \varepsilon)/2]^2},$$

$$q_7(y) = \frac{\varepsilon^2}{\varepsilon^2 - [y - ((3b/2) - c_2 + \varepsilon)/2]^2}, \quad q_8(y) = \frac{\varepsilon^2}{\varepsilon^2 - [y - ((3b/2) + c_2 - \varepsilon)/2]^2}.$$

The elements of the matrix for the inhomogeneous geometry of the cross section of **Figure 5a** are calculated in Fourier space by

$$
\begin{aligned}
g(n,m) = \frac{g_0}{ab} \Bigg\{ & \int_{((a/2)-d_1-\varepsilon)/2}^{((a/2)-d_1+\varepsilon)/2} \exp\left(1-q_1(x)\right) \cos\left(\frac{n\pi x}{a}\right) dx \\
& + \int_{((a/2)-d_1+\varepsilon)/2}^{((a/2)+d_1-\varepsilon)/2} \cos\left(\frac{n\pi x}{a}\right) dx + \int_{((a/2)+d_1-\varepsilon)/2}^{((a/2)+d_1+\varepsilon)/2} \exp\left(1-q_2(x)\right) \cos\left(\frac{n\pi x}{a}\right) dx \\
& + \int_{((3a/2)-d_2-\varepsilon)/2}^{((3a/2)-d_2+\varepsilon)/2} \exp\left(1-q_3(x)\right) \cos\left(\frac{n\pi x}{a}\right) dx \\
& + \int_{((3a/2)-d_2+\varepsilon)/2}^{((3a/2)+d_2-\varepsilon)/2} \cos\left(\frac{n\pi x}{a}\right) dx + \int_{((3a/2)+d_2-\varepsilon)/2}^{((3a/2)+d_2+\varepsilon)/2} \exp\left(1-q_4(x)\right) \cos\left(\frac{m\pi y}{b}\right) dx \Bigg\} \\
\Bigg\{ & \int_{((b/2)-c_1-\varepsilon)/2}^{((b/2)-c_1+\varepsilon)/2} \exp\left(1-q_5(y)\right) \cos\left(\frac{m\pi y}{b}\right) dy \\
& + \int_{((b/2)-c_1+\varepsilon)/2}^{((b/2)+c_1-\varepsilon)/2} \cos\left(\frac{m\pi y}{b}\right) dy + \int_{((b/2)+c_1-\varepsilon)/2}^{((b/2)+c_1+\varepsilon)/2} \exp\left(1-q_6(y)\right) \cos\left(\frac{m\pi y}{b}\right) dy \\
& + \int_{((3b/2)-c_2-\varepsilon)/2}^{((3b/2)-c_2+\varepsilon)/2} \exp\left(1-q_7(y)\right) \cos\left(\frac{m\pi y}{b}\right) dy \\
& + \int_{((3b/2)-c_2+\varepsilon)/2}^{((3b/2)+c_2-\varepsilon)/2} \cos\left(\frac{m\pi y}{b}\right) dy + \int_{((3b/2)+c_2-\varepsilon)/2}^{((3b/2)+c_2+\varepsilon)/2} \exp\left(1-q_8(y)\right) \cos\left(\frac{m\pi y}{b}\right) dy \Bigg\}.
\end{aligned}
$$

$$(9)$$

According to Ref. [19]. The cyclic matrix G is given by the form

$$
G = \begin{bmatrix}
g_{00} & g_{-10} & g_{-20} & \cdots & g_{-nm} & \cdots & g_{-NM} \\
g_{10} & g_{00} & g_{-10} & \cdots & g_{-(n-1)m} & \cdots & g_{-(N-1)M} \\
g_{20} & g_{10} & \ddots & \ddots & \ddots & & \\
\vdots & g_{20} & \ddots & \ddots & \ddots & & \\
g_{nm} & \ddots & \ddots & \ddots & g_{00} & & \vdots \\
\vdots & & & & & & \\
g_{NM} & \cdots & \cdots & \cdots & \cdots & \cdots & g_{00}
\end{bmatrix}
$$

$$(10)$$

Similarly, the $\mathbf{G_x}$ and $\mathbf{G_y}$ matrices are obtained by the derivatives of the Fourier components of the dielectric profile. These matrices relate to the method that based on the Laplace and Fourier transforms, the inverse Laplace and Fourier transforms [19].

The proposed technique to calculate the elements of the matrix **G** relates to the method [19]. This method becomes an improved method by using the proposed technique also for discontinuous problems of the hollow rectangular waveguide.

5. Numerical results

This section presents several examples for the different geometries in the cross section. Five examples of the different discontinuous cross sections and complementary shapes are demonstrated in **Figure 1a–e**. All the next graphical results are

demonstrated as a response to a half-sine (TE_{10}) input-wave profile and the inhomogeneous geometries of the cross section.

Figure 7a–e shows the results of the output field as a response to a half-sine (TE_{10}) input-wave profile for the rectangular dielectric profile (**Figure 4a**) in the rectangular cross section for ϵ_r = 3, 5, 7, and 10, respectively, where a = b = 20 mm, and c = d = 5 mm. The center of the dielectric rectangle is located in the center of the cross section at the point (a/2, b/2), where ϵ_r = 3, 5, 7, and 10, respectively. The output field in the same cross section of **Figure 7a–d** is shown in **Figure 7e** for the x-axis where y = b/2 = 10 mm, where ϵ_r = 3, 5, 7, and 10, respectively. The other parameters are z = 15 cm, k_0 = 167 $1/m$, λ = 3.75 cm, and β = 58 $1/m$.

The results of **Figure 7a–e** are demonstrated for ϵ_r = 3, 5, 7, and 10, respectively. The results are strongly affected by the half-sine (TE_{10}) input-wave profile, and the location of the center of the dielectric material.

The output field for the hollow rectangular waveguide where the dielectric material is located between the hollow rectangle and the metal is shown in
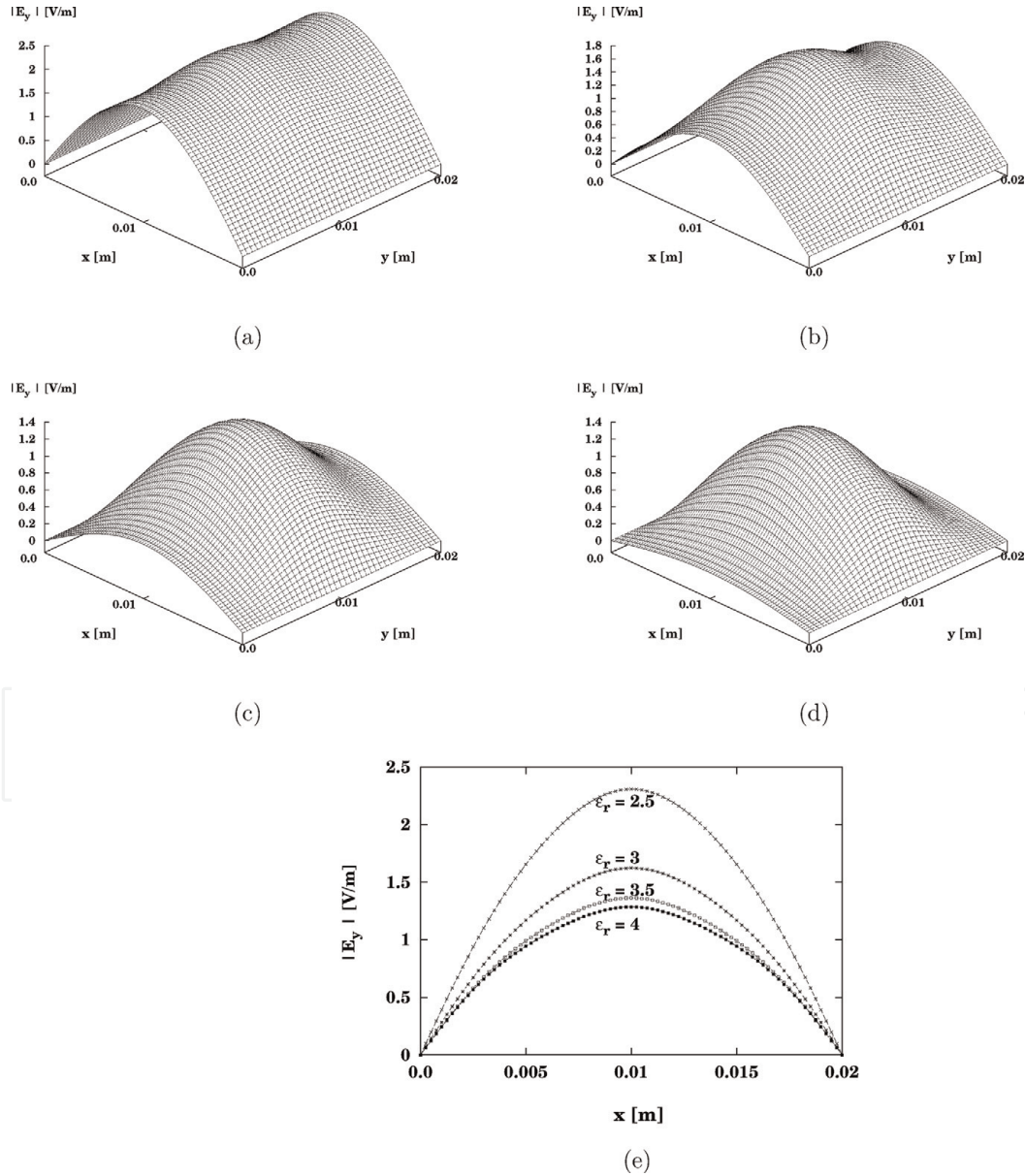

(a)

(b)

(c)

(d)

(e)
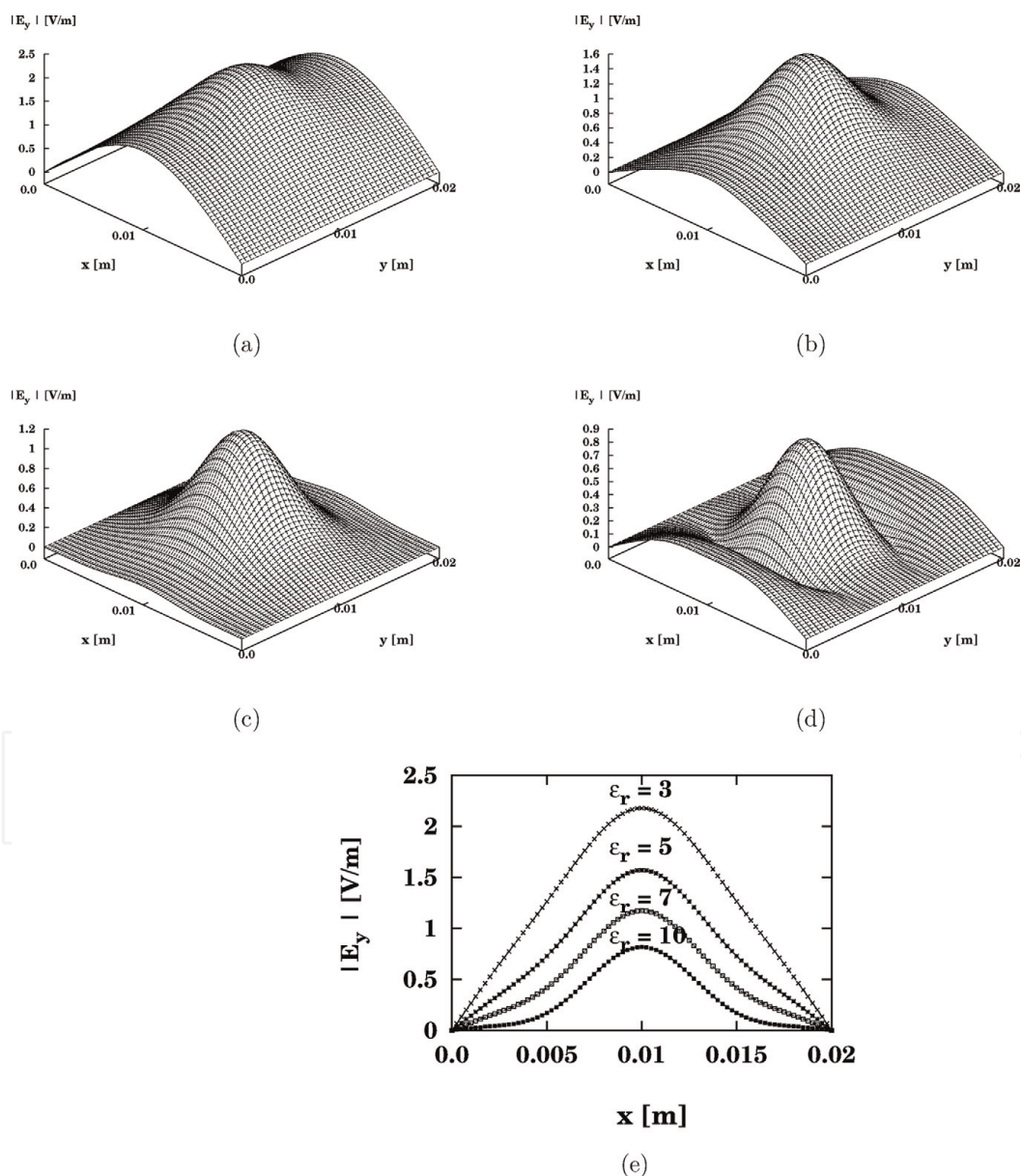
Figure 7.
The output field as a response to a half-sine (TE₁₀) input-wave profile for the rectangular dielectric profile Figure 4a in the rectangular cross section, where a = b = 20 mm, and c = d = 5 mm. The center of the rectangle dielectric profile is located in the center of the cross section, for (a) ϵ_r = 3, for (b) ϵ_r = 5, for (c) ϵ_r = 7, and for (d) ϵ_r = 10. (e). The output field in the same cross section of the results (a–d) for x-axis and where y = b/2 = 10 mm, for the values of ϵ_r = 3, 5, 7, and 10, respectively.

Figure 8a–d, where a = b = 20 mm, and c = d = 14 mm. In this case the thickness of the dielectric layer is equal to 3 mm (e = f = 3 mm). The results are demonstrated for $\epsilon_r = 2.5$, $\epsilon_r = 3$, $\epsilon_r = 3.5$, and $\epsilon_r = 4$, respectively. The output field in the same cross section of **Figure 8a–d** is shown in **Figure 8e**, for $\varepsilon_r = 2.5$, 3, 3.5, and 4, respectively, for x-axis where y = b/2 = 10 mm. In this case, z = 15 cm, $k_0 = 167$ 1/m, $\lambda = 3.75$ cm, and $\beta = 58$ 1/m. These results are shown for $\epsilon_r = 2.5$, 3, 3.5, and 4, respectively, and these results are strongly affected by the half-sine (TE_{10}) input-wave profile, the location of the center of the dielectric material, and the thickness of the dielectric material between the hollow rectangle and the metal.

We can find the relevant parameters to obtain the Gaussian behavior of the output field. We can show that the Gaussian behavior is obtained when the thickness of the dielectric layer is equal to 3 mm, as shown in the results of **Figure 8a–d**. The output results are strongly affected by the thickness of the dielectric layer.

Figure 9a–d shows the results of the output field as a response to a half-sine (TE_{10}) input-wave profile for the cross section with four dielectric profiles, as

(a)

(b)

(c)

(d)

(e)

Figure 8.
*The output field as a response to a half-sine (TE$_{10}$) input-wave profile for the hollow rectangular waveguide where the hollow rectangle is located in the center of the cross section **Figure 4b**, where a = b = 20 mm, c = d = 14 mm. The thickness of the dielectric layer is equal to 3 mm (e = f = 3 mm). The results are shown for (a) ϵ_r = 2.5, for, (b) ϵ_r = 3, for, (c) ϵ_r = 3.5, and for, (d) ϵ_r = 4, (e) the output field in the same cross section of the results (a–d) is shown for x-axis and where y = b/2 = 10 mm, for ϵ_r = 2.5, 3, 3.5, and 4, respectively.*
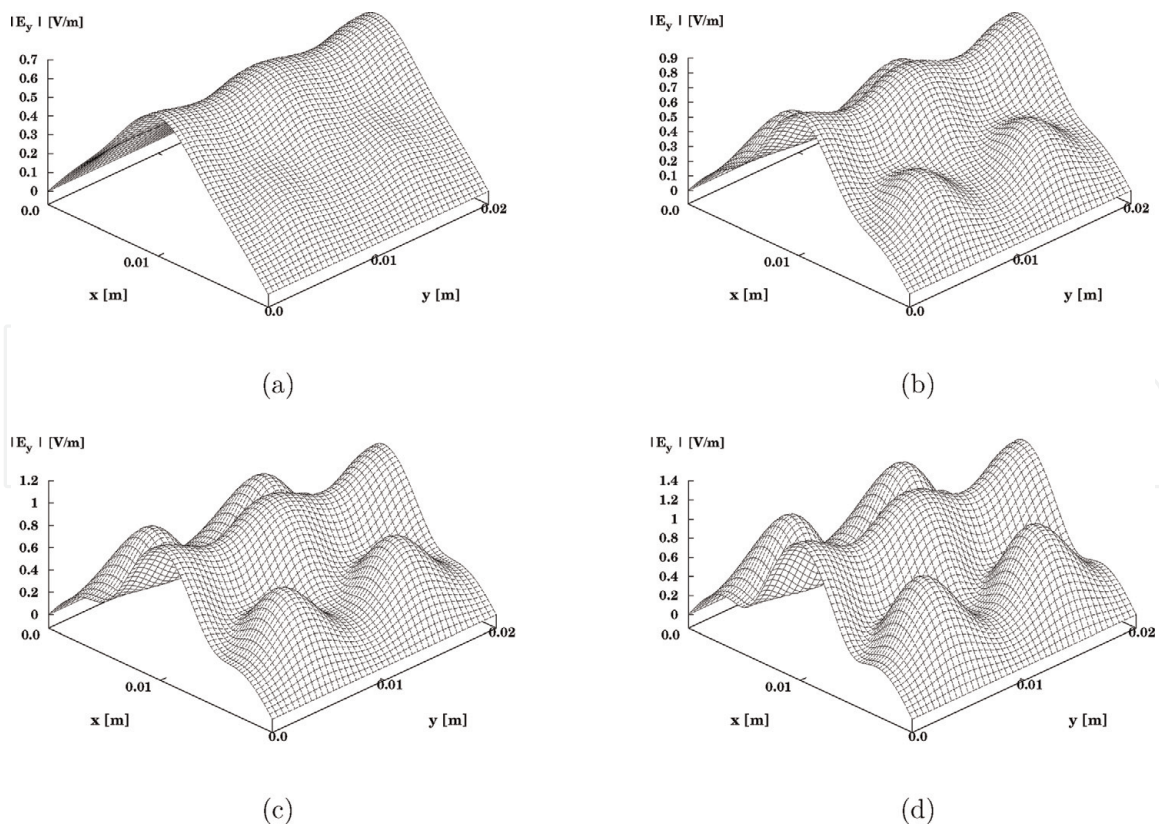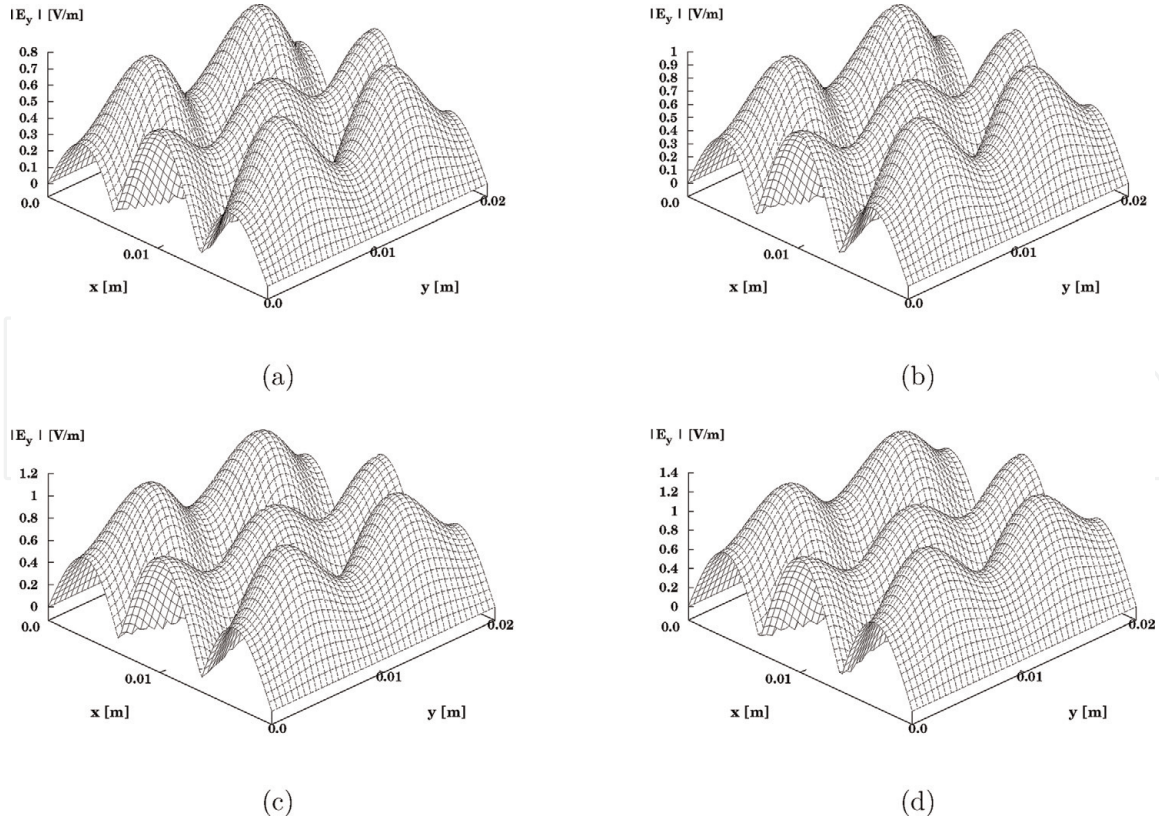
Figure 9.
*The output field as a response to a half-sine (TE$_{10}$) input-wave profile for the cross section with four dielectric profiles, as shown in **Figure 5a**. The centers of the first, the second, the third and the firth dielectric rectangles are located at the points (a/4, b/4), (3a/4, b/4), (a/4, 3b/4), and (3a/4, 3b/4), respectively. The parameters are a = b = 20 mm, c = d = 0.4 mm, and z = 15 cm, where (a). ϵ_r = 1.1; (b). ϵ_r = 1.2; (c). ϵ_r = 1.3; (d). ϵ_r = 1.4.*

shown in **Figure 5a**. In this example we suppose that a = b = 20 mm, c = d = 0.4 mm, z = 15 cm, the centers of the first, the second, the third, and the firth dielectric rectangles are located at the points (a/4, b/4), (3a/4, b/4), (a/4, 3b/4), and (3a/4, 3b/4), respectively, and for ε_r = 1.1, 1.2, 1.3 and 1.4, respectively. The other parameters are k_0 = 167 1/m, λ = 3.75 cm and β = 58 1/m. By increasing the parameter ϵ_r from 1.1 to 1.4, the output dielectric profile increased, the output profile of the half-sine (TE$_{10}$) profile decreased, and the output amplitude increased. These results are strongly affected by the half-sine (TE$_{10}$) input-wave profile, and the locations of the rectangular profiles along x-axis and y-axis.

Figure 10a–d shows the results of the output field as a response to a half-sine (TE$_{10}$) input-wave for the hollow waveguide with four hollow rectangles, where a = b = 20 mm, c = d = 3.3 mm, and z = 15 cm, ϵ_r = 1.2, 1.3, 1.4, and 1.5, respectively. The centers of the first, the second, the third and the firth hollow rectangles are located at the points (a/4, b/4), (3a/4, b/4), (a/4, 3b/4), and (3a/4, 3b/4), respectively. The other parameters are k_0 = 167 1/m, λ = 3.75 cm and β = 58 1/m. These results are strongly affected by the half-sine (TE$_{10}$) input-wave profile, and the locations of the rectangular profiles along x-axis and y-axis.

By increasing only the parameter ϵ_r, the output dielectric profile increased, the output profile of the half-sine (TE$_{10}$) profile decreased, and the output amplitude increased. These results are strongly affected by the half-sine (TE$_{10}$) input-wave profile, and the locations of the rectangular profiles along x-axis and y-axis.

The applications are useful for straight waveguides in millimeter regimes, in the cases where the dielectric profile is located in the center of the cross section, for the cases where the hollow rectangle is located in the center of the cross section, and also for complicated and discontinuous profiles in the cross section.

(a)

(b)

(c)

(d)

Figure 10.
*The output field as a response to a half-sine (TE_{10}) input-wave profile for the hollow waveguide with four hollow rectangles, as shown in **Figure 5b**. The centers of the first, the second, the third and the firth hollow rectangles are located at the points (a/4, b/4), (3a/4, b/4), (a/4, 3b/4), and (3a/4, 3b/4), respectively. The parameters are a = b = 20 mm, c = d = 3.3 mm, and z = 15 cm, where hollow waveguide with four hollow rectangles, as shown in **Figure 1e**, (a). ϵ_r = 1.5; (b). ϵ_r = 2; (c). ϵ_r = 2.5; (d). ϵ_r = 3.*

6. Conclusions

This chapter presents two interesting types of dielectric materials in the straight rectangular waveguides and their applications. Five examples of the different discontinuous cross section were demonstrated. The effective technique was proposed for all case of **Figure 1a–e**, in order to calculate the dielectric material in the specific cross section.

The proposed techniques are very important to understand the influence of the dielectric materials and the hollow rectangles in all case of discontinuous geometry in the cross section. All the graphical results are demonstrated as a response to a half-sine (TE_{10}) input-wave profile. The proposed techniques relate to the method based on Laplace and Fourier transforms and the inverse Laplace and Fourier transforms.

The method is based on Fourier transform, thus we need use with the image method to calculate the dielectric profile in the cross section. The image method and periodic replication are needed for fulfilling the boundary condition of the metallic waveguide.

Figure 8a–e relates to the hollow rectangular waveguide where the hollow rectangle is located in the center of the cross section as shown in **Figure 4b**. We can find the relevant parameters to obtain the Gaussian behavior of the output field. From the results of **Figure 8a–e**, the Gaussian behavior is obtained when the thickness of the dielectric layer is equal to 3 mm. The output results are strongly affected by the thickness of the dielectric layer.

By increasing only the parameter ϵ_r, the output dielectric profile increased, the output profile of the half-sine (TE_{10}) profile decreased, and the output amplitude

increased. The results are strongly affected by the half-sine (TE_{10}) input-wave profile, the location of the center of the dielectric material, and the thickness of the dielectric material between the hollow rectangle and the metal.

The applications are useful for straight waveguides in millimeter regimes, in the cases where the dielectric profile is located in the center of the cross section, for cases where the hollow rectangle is located in the center of the cross section, and also for complicated and discontinuous profiles in the cross section.

Author details

Zion Menachem
Department of Electrical Engineering, Sami Shamoon College of Engineering,
Beer Sheva, Israel

*Address all correspondence to: zionme@sce.ac.il; zionmm@gmail.com

IntechOpen

References

[1] Chiang KS. Review of numerical and approximate methods for the modal analysis of general optical dielectric waveguides. Optical and Quantum Electronics. 1994;**26**:S113-S134

[2] Saad M. Review of numerical methods for the analysis of arbitrarily-shaped microwave and optical dielectric waveguides. IEEE Transactions on Microwave Theory and Techniques. 1985;**MTT-33**:894-899

[3] Yeap KH, Teh KH, Yeong KC, Lai KC, Loh MC. Propagation in dielectric rectangular waveguides. Optica Applicata. 2016;**XLVI**:317-330

[4] Bartling JQ. Propagation of an electromagnetic wave in an infinite rectangular dielectric wave guide. Journal of the Franklin Institute. 1969;**287**:389-407

[5] Khorasani S. Differential transfer-matrix method for solution of one-dimensional linear nonhomogeneous optical structures. Optical Society of America. 2003;**20**:91-96

[6] Rojas JAM, Alpuente J, Pineiro J, Sanchez R. Rigorous full vectorial analysis of electromagnetic wave propagation in 1D inhomogeneous media. Progress in Electromagnetics Research. 2006;**63**:89-105

[7] Mehrany K, Khorasani S. Analytical solution of non-homogeneous anisotropic wave equations based on differential transfer matrices. Journal of Optics A. 2002;**4**:624-635

[8] Lee JF. Finite element analysis of lossy dielectric waveguides. IEEE Transactions on Microwave Theory and Techniques. 1994;**42**:1025-1031

[9] Ise K, Inoue K, Koshiba M. Three-dimensional finite-element method with edge elements for electromagnetic waveguide discontinuities. IEEE Transactions on Microwave Theory and Techniques. 1991;**39**:1289-1295

[10] Singh V, Joshi M, Prasad B, Ojha P. Modal dispersion characteristics and waveguide dispersion of an optical waveguide having a new unconventional core cross-section. Journal of Electromagnetic Waves and Applications. 2004;**18**:455-468

[11] Hernandez-Lopez MA, Quintillan M. Propagation characteristics of modes in some rectangular waveguides using the finite-difference time-domain method. Journal of Electromagnetic Waves and Applications. 2000;**14**:1707-1722

[12] Mallick AK, Sanyal GS. Electromagnetic wave propagation in a rectangular waveguide with sinusoidally varying width. IEEE Transactions on Microwave Theory and Techniques. 1978;**MTT-26**:243-249

[13] Bogle A, Havrilla M, Nyquis D, Kempel L, Rothwell E. Electromagnetic material characterization using a partially-filled rectangular waveguide. Journal of Electromagnetic Waves and Applications. 2005;**19**:1291-1306

[14] Vaish A, Parthasarathy H. Analysis of a rectangular waveguide using finite element method. Progress in Electromagnetics Research C. 2008;**2**:117-125

[15] Khalaj-Amirhosseini M. Analysis of longitudinally inhomogeneous waveguides using the method of moments. Progress In Electromagnetics Research. 2007;**74**:57-67

[16] Khalaj-Amirhosseini M. Analysis of nonuniform transmission lines using Taylor's series expansion. International

Journal of RF and Microwave
Computer-Aided Engineering. 2006;**10**:
536-544

[17] Molina-Fernandez I, Camacho-
Penalosa C, Ramos JI. Application of the
two-dimensional Fourier transform to
nonlinear wave propagation
phenomena. IEEE Transactions on
Microwave Theory and Techniques.
1994;**42**:1079-1085

[18] Henry CH, Verbeek BH. Solution of
the scalar wave equation for arbitrarily
shaped dielectric waveguides by two-
dimensional Fourier analysis. Journal of
Lightwave Technology. 1989;**7**:308-313

[19] Menachem Z, Jerby E. Transfer
matrix function (TMF) for propagation
in dielectric waveguides with arbitrary
transverse profiles. IEEE Transactions
on Microwave Theory and Techniques.
1998;**46**:975-982

[20] Vladimirov V. Equations of
Mathematical Physics. New York, NY:
Marcel Dekker; 1971